Catalytic Behavior of Chromium Oxide Supported on Nanocasting-Prepared Mesoporous Alumina in Dehydrogenation of Propane

Adam Węgrzyniak [1], Sebastian Jarczewski [2], Adam Węgrzynowicz [1], Barbara Michorczyk [1], Piotr Kuśtrowski [2] and Piotr Michorczyk [1,*

[1] Institute of Organic Chemistry and Technology, Cracow University of Technology, Warszawska 24, 31-155 Kraków, Poland; wegrzyniak@indy.chemia.pk.edu.pl (A.W.); vinnicki@chemia.pk.edu.pl (A.W.); bmichorczyk@indy.chemia.pk.edu.pl (B.M.)

[2] Faculty of Chemistry, Jagiellonian University, Gronostajowa 2, 30-387 Kraków, Poland; jarczewski@chemia.uj.edu.pl (S.J.); kustrows@chemia.uj.edu.pl (P.K.)

* Correspondence: pmichor@pk.edu.pl; Tel.: +48-12-628-27-51

Abstract: Mesoporous alumina with narrow pore size distribution centered in the range of 4.4–5.0 nm and with a specific surface area as high as 270 $m^2 \cdot g^{-1}$ was prepared via the nanocasting approach using a CMK-3 carbon replica as a hard template. Based on this support, a series of catalysts containing 1, 5, 10, 20 and 30 wt % of chromium was prepared by incipient wetness impregnation, characterized, and studied in the dehydrogenation of propane to propene (PDH). Cr species in three oxidation states—Cr(III), Cr(V) and Cr(VI)—were found on the oxidized surface of the catalysts. The concentration of these species varied with the total Cr loading. Temperature-programmed reduction (H_2-TPR) and UV-Vis diffuse reflectance spectroscopy (UV-Vis-DRS) studies revealed that Cr(VI) species dominated at the lowest Cr content. An increase in the Cr loading resulted in an appearance of an increasing amount of Cr(III) oxide. UV-Vis-DRS measurements performed in situ during the PDH process showed that at the beginning of the catalytic test Cr(VI) species were reduced to Cr(III) redox species. A crucial role of the redox species in the PDH process over the catalysts with the low Cr content was confirmed. The stability test for the catalyst containing 20 wt % of Cr showed that this sample exhibited the reproducible catalytic performance after the first four regeneration–dehydrogenation cycles. Moreover, this catalyst had higher resistance on deactivation during the PDH process as compared to the reference catalyst with the same Cr loading, but was supported on commercially available alumina.

Keywords: nanocasting; chromium–aluminum catalysts; propane dehydrogenation; propylene

1. Introduction

Propylene can be obtained from propane by non-oxidative or oxidative dehydrogenation pathways [1–4]. The oxidative dehydrogenation of propane has not been commercialized yet, mainly due to problems with the control of selectivity with reasonable propane conversion (too much thermodynamically-favored CO_x is usually formed). Some alternative processes, in which oxygen is replaced by weaker oxidizing agents (such as carbon dioxide), have been under investigation [3–9]. On the other hand, non-oxidative dehydrogenation of propane to propylene (PDH) is nowadays one of the most important forms of on-purpose technology for propylene production. Three type of PDH technologies—CATOFIN (Lummus Technology), Oleflex (UOP) and STAR (ThyssenKrupp Uhde)—have been developed on an industrial scale in more than 14 installations. Dozens of the new installations are already under construction or have been announced [3].

Despite the quite simple chemistry of PDH, the industrial implementation of this process is very complicated due to side reactions, such as cracking, polymerization, hydrogenolysis and coke formation. Important aspects in the PDH process are: (1) achievement of high per-pass conversion (near equilibrium conversion) and (2) limitation of side reactions and coke formation. Therefore, many efforts have continued to focus on the improvement of process configuration and catalyst formulation.

In commercialized PDH technologies, platinum- and chromium-based catalysts are widely applied [1,3,4]. Many other promising catalytic systems that are less hazardous for the environment than chromium or cheaper than platinum are being investigated, and are based on vanadium [10–12], gallium [13,14], iron [15,16], tungsten [17] or indium [18] oxides. In most cases, catalytically active compounds are deposited on supports characterized by a large specific surface area and accessible pore system. Moreover, promoters are added in order to enhance either selectivity or stability. For example, in the CATOFIN process, the γ-Al_2O_3-supported catalyst containing 18–20 wt % of CrO_x is doped with 1–2 wt % of K or Na [3].

In the case of Cr-containing catalysts, many factors, including the type of precursors, Cr loading, and the preparation procedure as well as the support nature, influence the distribution of Cr species at various oxidation states, which has a direct impact on the catalytic performance in the PDH process [19–26]. In oxidized alumina-supported chromium oxide catalysts, chromium is stabilized in three oxidation states—Cr(III), Cr(V) and Cr(VI) [19,21,24]. During the dehydrogenation process these species form redox and non-redox Cr(III) sites. The former species arise due to the reduction of Cr(V) and Cr(VI) species in the initial period of the dehydrogenation process, while non-redox Cr(III) species originate from highly stabilized Cr(III) existing on the surface of the fresh catalyst [21,27,28]. It has been recognized that the presence of Cr(III) redox sites is crucial for high activity of the PDH catalyst [21,29,30]. The correlation between the number of redox Cr sites and activity is observed especially at low Cr loadings. At higher Cr contents, the impact of non-redox species on the catalytic activity cannot be neglected. Assuming the crucial role of Cr redox species in propane dehydrogenation, much attention has been paid to the selection of support with chemical properties and surface areas suitable for achieving a high contribution of redox Cr sites with a Cr loading as high as possible [31,32]. From this point of view, mesoporous supports, which offer high surface area and resistance to pore blocking (for instance by coke formed during catalytic runs), were found to be attractive. Very promising results were observed in the case of siliceous mesoporous materials with different pore architectures and surface areas [5,9,31,32]. For example, in propane dehydrogenation in the presence of CO_2 we found that an increase in a specific surface area of silica by the application of mesoporous supports (SBA-15, SBA-1) increases the number of available Cr redox species and results in better PDH performance at high Cr loading [32].

In this work, we focused on the application of ordered mesoporous alumina instead of commercial alumina as a support for chromium oxide in a PDH catalyst. Various methods of synthesis of mesoporous alumina, with a surface area of 200–400 $m^2 \cdot g^{-1}$ and mesoporosity in the range 2–10 nm, were elaborated using different soft and hard templates, preparation procedures and precursors [33–37]. Herein, we used the nanocasting approach based on carbon hard templates (CMK-3) with the rod-type structure obtaining alumina with the hexagonal mesopore arrangement [35,37]. Using this alumina support we subsequently prepared catalysts containing 1–30 wt % of Cr_2O_3, which were characterized and tested in the dehydrogenation of propane to propene.

2. Results

2.1. Characterization of Alumina Support

The nanocasting route was applied for the preparation of pure Al_2O_3. Table 1 summarizes low-temperature nitrogen adsorption results for the hard templates (SBA-15 and CMK-3) as well as for the alumina support calcined at the various temperatures in air. The samples of alumina annealed between 600 and 800 °C are characterized by relatively high specific surface areas, which vary in the

range of 250–270 $m^2 \cdot g^{-1}$, and narrow mesoporous-size distributions centered in the range of 4.4–5.0 nm (Figure S1). The thermal treatment at 900 °C brings about a significant reduction of specific surface area as well as broadening of the Barrett–Joyner–Halenda(BJH)pore size distribution. Moreover, in the samples calcined at 800 and 900 °C, the γ-Al_2O_3 phase appears (Figure S2). The phase transformation at high temperature ($\geq$800 °C) is in a good agreement with results reported for mesoporous alumina prepared by the hard template approach [34]. Taking into account criteria of enhanced porosity and thermal stability under the conditions of the PDH process (typically 550–600 °C) a calcination temperature as high as 700 °C seems to be reasonable for the final thermal treatment of Al_2O_3-n.

Table 1. Phase composition and textural properties of SBA-15, CMK-3 and mesoporous supports obtained by nanocasting. S_{BET}: specific surface area; V_{micro}: micropore pore volume; V_{meso}: mesopore volume; V_{total}: total pore volume.

Sample	Calcination/Pretreatment Temperature (°C)	Phase Composition	S_{BET} $(m^2 \cdot g^{-1})$	V_{micro} $(cm^3 \cdot g^{-1})$	V_{meso} $(cm^3 \cdot g^{-1})$	V_{total} $(cm^3 \cdot g^{-1})$
SBA-15 [a]	550	-	756	0.01	0.83	0.84
CMK-3 [a]	800	-	1411	0.10	1.22	1.23
Al_2O_3-n	600	-	259	0.01	0.32	0.33
	700	-	270	0.00	0.41	0.41
	800	γ-Al_2O_3	254	0.00	0.44	0.44
	900	γ-Al_2O_3	178	0.02	0.35	0.37

[a] data from [37].

However, it should be noted that in comparison to SBA-15 (initial hard silica template), the Al_2O_3-n nanoreplicas have wider pore size distribution with a tail at larger pore sizes. Moreover, in the case of Al_2O_3-n nanoreplicas the maxima of pore size distribution and d_{100} values are lower than for SBA-15. For instance, in the case of Al_2O_3-n calcined at 700 °C the pore size maximum and the d_{100} values are 4.7 and 7.5 nm, and for SBA-15 these values are 8.1and 9.2 nm, respectively. Such changes of these parameters can be explained by the structural shrinkage process of carbon framework during the CMK-3 preparation as was reported previously [37].

Ordered pore structure and morphology of Al_2O_3-n calcined at 700 °C were confirmed by transmission electron microscopy (TEM) and scanning electron microscopy (SEM) analysis (Figure 1). As we reported previously, SBA-15 and its negative carbon replica (CMK-3) consist of wheat-like aggregates with rope-like domains characterized by a uniform size of about 1 µm [32].
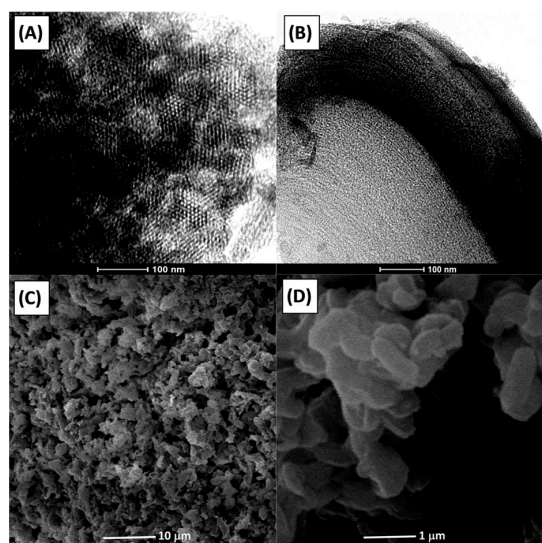

Figure 1. TEM (**A**,**B**) and SEM (**C**,**D**) images of Al_2O_3-n calcined at 700 °C.

Particles of Al$_2$O$_3$-n have similar shapes indicating that after replication the morphology of the initial rigid template is preserved (Figure 1C,D). The TEM micrographs (Figure 1A,B) indicate that the double replication results in a decrease of long-range structural order in comparison with the rigid templates (CMK-3 and SBA-15).

2.2. Characterization of Catalysts

Based on ordered mesoporous alumina calcined at 700 °C, a series of Crx/Al$_2$O$_3$-n catalysts were prepared with Cr loadings very close to those expected (Table 2). Figure 2 displays the X-ray diffraction (XRD) patterns collected for the calcined catalysts in the 2 theta range of 1–5°. The patterns of the samples containing between 1 and 20 wt % of Cr$_2$O$_3$ exhibit (100) reflection, which indicates the preservation of the hexagonal pore arrangement of the initial hard template (SBA-15) after repeated templating and impregnation. The intensity of the reflection decreases rapidly with the increase of the Cr content. The progressive reduction of the intensity of (100) reflection with the increase in the Cr loading is more likely due to a dilution of alumina by chromium introduced during impregnation as a consequence of its higher absorption factor for X-rays compared to alumina.

Table 2. Base characterization of Crx/Al$_2$O$_3$-n catalysts.

Sample	Cr$_{tot}$ Content [a] (wt % of Cr$_2$O$_3$)	H$_2$-TPR		NH$_3$-TPD (μmol NH$_3$·m^{-2}) [b]			S$_{BET}$ (m^2·g^{-1})	V$_{total}$ (cm^3·g^{-1})
		H$_2$ mmol·g^{-1}	H$_2$/Cr$_{tot}$	Weak	Medium-Strong	Total		
Cr1/Al$_2$O$_3$-n	1.2	0.16	1.34	0.26	1.31	1.57	232	0.36
Cr5/Al$_2$O$_3$-n	5.1	0.67	0.94	0.43	1.93	2.36	175	0.23
Cr10/Al$_2$O$_3$-n	10.1	1.33	0.54	0.31	2.02	2.33	170	0.12
Cr20/Al$_2$O$_3$-n	22.5	2.96	0.27	0.63	2.23	2.87	148	0.13
Cr30/Al$_2$O$_3$-n	28.7	3.78	0.25	0.59	1.31	1.90	129	0.12

[a] Total Cr content calculated by inductively-coupled plasma (ICP) in wt % of Cr$_2$O$_3$. [b] Number of acid sites estimated based on deconvolution of NH$_3$-TPD profiles (Figure S4).
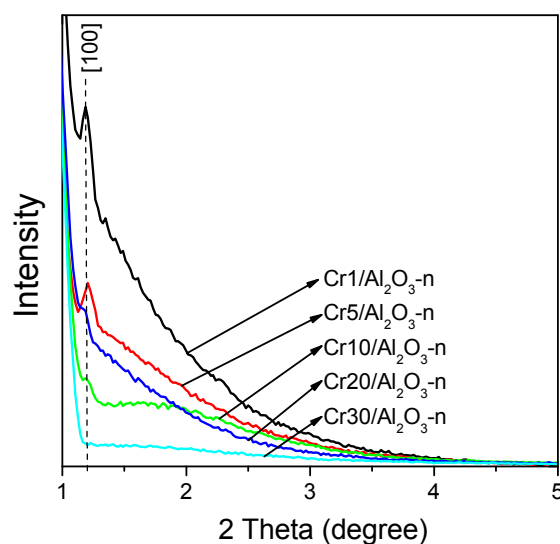

Figure 2. X-ray diffraction patterns of chromium oxide catalysts.

The maintenance of the ordered cubic arrangement of Al$_2$O$_3$-n frameworks upon deposition of chromium is further supported by the low-temperature N$_2$ adsorption data. The isotherms and BJH mesopore distributions are displayed in Figure S3, whereas the textural parameters, such as specific surface area (S_{BET}) and total pore volume (V_{total}), are presented in Table 2.

The S_{BET} and V_{total} decrease with the increase in the Cr$_{tot}$ content, confirming a gradual filling of the pore system with chromium oxide. The deposition of 30 wt % of Cr$_2$O$_3$ results in a significant decrease in S_{BET} of about 50% in comparison to the parent Al$_2$O$_3$-n. Moreover, the Cr deposition also

has an impact on pore size distribution (Figure S3). With the increase in the Cr content the maximum of pore size distribution shifts to lower values, that can be explained by the deposition of chromium species inside the pores.

The oxidation state of Cr in the deposited species, reducibility and phase composition were subjected to careful investigation of the calcined Crx/Al$_2$O$_3$-n catalysts by temperature-programmed reduction (H$_2$-TPR), UV-Vis-DRS, XRD and electron paramagnetic resonance (EPR) (Figure 3).
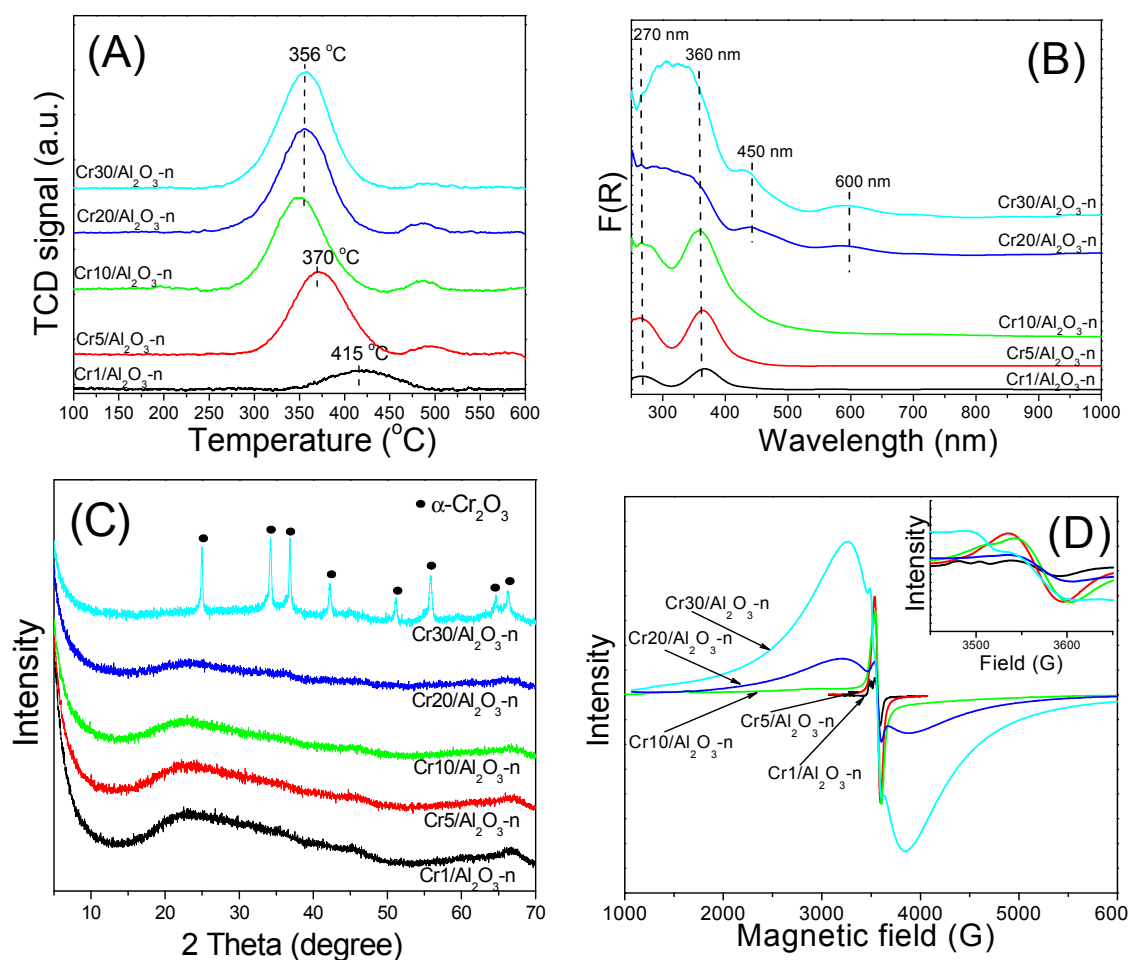

Figure 3. H$_2$-TPR profiles (**A**); UV-Vis DRS spectra (**B**); XRD patterns (**C**); and electron paramagnetic resonance (EPR) spectra (**D**) measured for Crx/Al$_2$O$_3$-n catalysts.

The H$_2$-TPR profiles of all catalysts show only one reduction maximum in the temperature range from 356 to 415 °C (Figure 3A). In the case of chromium-alumina samples, this single peak related to hydrogen consumption is assigned to reduction of Cr(VI) to Cr(III) [20,21]. Its position shifts to lower temperature with an increase of the Cr content from 1 to 10 wt %, indicating changes in the dispersion of the Cr(VI) species. At higher Cr contents (>10 wt %), this maximum is found at the similar positions due to insignificant changes in the dispersion of Cr (VI) species. Table 2 summarizes the quantitative results of the H$_2$-TPR measurements. The H$_2$ consumption increases with the Cr loading up to 5 wt % of Cr$_2$O$_3$ and then only slightly for the catalysts with the higher Cr content, whereas the H$_2$/Cr$_{tot}$ ratio drops rapidly from 1.35 to 0.27 as the Cr loading is increased from 1 to 30 wt % of Cr$_2$O$_3$. In the case of the sample with the lowest Cr content, the H$_2$/Cr$_{tot}$ is close to the value of 1.5, which corresponds to theoretical reduction of Cr(VI) to Cr(III) species (2CrO$_3$ + 3H$_2$ = Cr$_2$O$_3$ + 3H$_2$O). For higher Cr contents the H$_2$/Cr$_{tot}$ ratio is considerably lower. This indicates that above monolayer coverage of the support non-redox Cr sites are produced predominantly. A similar drop in the H$_2$/Cr$_{tot}$ ratio with the increase

in the Cr loading was described for chromium oxide systems deposited on commercial alumina [21], titania [21] as well as on ordered and unordered mesoporous silicas [21,28,32].

The presence of Cr(VI) and Cr(III) species on the surface of the fresh catalysts confirms UV-Vis-DRS studies as well (Figure 3B). For all catalysts absorption bands at 270 and 360 nm are distinguished, which can be assigned to the O→Cr^{6+} charge transfer transitions in monochromate species. Specifically, the bands at 270 nm and 360 nm are due to the transitions $^1A_1 \rightarrow {}^1T_2$ ($1t_1 \rightarrow 7t_2$ and $6t_2 \rightarrow 2e$) and $^1A_1 \rightarrow {}^1T_2$ ($1t_1 \rightarrow 2e$), respectively [38,39].

Additionally, the spectra of the catalysts with the Cr content above 10 wt % show a shoulder about 450 nm and the broad band at 600 nm. The former band corresponds to either Cr_2O_3 or the dichromate/polymeric species (with low symmetry), while the band at 600 nm is attributed to d-d transitions of Cr^{3+} ($^4A_{2g} \rightarrow {}^4T_{2g}$) in octahedral symmetry, as in Cr_2O_3 particles [38].

The formation of the Cr_2O_3 phase is also evidenced by XRD (Figure 3C). In the 2θ range of $10°$–$70°$, the diffraction lines corresponding to the crystal phase of α-Cr_2O_3 are presented only in the XRD pattern of the sample with the highest Cr content (Cr30/Al_2O_3-n). The absence of the diffraction lines characteristic of the α-Cr_2O_3 phase in the XRD patterns of the catalysts with lower Cr loadings can be explained by high dispersion of this phase inside the mesopores of alumina support, which suppresses agglomeration during the preparation of the catalyst. We have previously reported very similar dispersion for materials based on mesoporous silicas, such as MCM-41, SBA-1 or SBA-15 [5,28,32].

The average crystallite size of the α-Cr_2O_3 phase detected in the Cr30/Al_2O_3-n catalyst was estimated using the Scherrer's equation (D = $(0.89 \times \lambda)/(\beta \times \theta)$), where: D—average crystallite size, 0.89—dimensionless shape factor, λ—X-ray wavelength, β—line broadening at half maximum intensity, and θ—diffraction angle. The estimated average crystallite size of α-Cr_2O_3 was equal to 32 nm, indicating that at very high Cr loading (30 wt %), presumably also larger crystals are formed outside the pore systems.

Figure 3D shows the EPR spectra of the Crx/Al_2O_3-n catalysts. In the case of the studied chromium oxide materials, three main EPR signals are observed. The γ-signal with a linewidth of 3.5–6.0 mT at around g = 1.97 originates from the isolated Cr^{5+} species. The β-signal with a linewidth of about 78–85 mT and g = 1.99 is assigned to Cr^{3+} species in nearly octahedral coordination in small clusters. The third δ-signal, corresponding to the isolated Cr^{3+} species [39], consists of a broad line centered at about g = 1.9–2.2 and a positive lobe at about g = 2.5–4.5 [24]. For the Crx/Al_2O_3-n catalysts, the γ-signal characteristic of Cr^{5+} species with the position of g = 1.97–1.98 and a linewidth in the range of 4–7 mT was observed. Moreover, in the samples with the Cr content ≥20 wt %, the additional broad β-signal originating from the agglomerated Cr^{3+} species appeared. For the same samples, the presence of UV-Vis DRS band at 600 nm confirms the EPR findings.

Changes in surface acidity after the Cr deposition on the Al_2O_3-n support were studied by temperature-programmed desorption of ammonia (NH_3-TPD). The NH_3-TPD profiles for Al_2O_3-n and the Crx/Al_2O_3-n catalysts consist of a peak at ca. 170–180 °C followed by a peak with the maximum in the range of 290–310 °C and an overlapping peak at ca. 450 °C (Figure S4). The quantitative data on the acidity were obtained on the basis of mathematical deconvolution of the experimental TPD curves and by assigning the peaks with maxima at 190 °C to desorption of NH_3 bonded by weak acid sites and those at 310 and 450 °C to the deliberation of medium–strong acid sites. The concentration of weak, medium–strong, and total number of acid sites normalized to the specific surface area are reported in Table 2.

It is generally accepted that various alumina supports, including also mesoporous alumina, have solely Lewis acid sites [10]. As is shown the deposition of chromium has influence on both distribution and total concentration of acid sites. The concentration of strong-medium acid sites rises with the Cr content up to 20 wt % of Cr_2O_3, and then for the sample with the highest Cr content, it declines.

2.3. Catalytic Properties of Cr-Containing Samples

2.3.1. Effect of the Nature of Cr

First, the catalytic performance of the Crx/Al$_2$O$_3$-n materials with different Cr loadings was examined in the PDH process. The initial specific activity, conversion of propane, yield of propene, as well as selectivity to propene, ethane, ethene and methane are summarized in Table 3, while variations of propane conversion and selectivity to propene vs. time-on-stream over the Crx/Al$_2$O$_3$-n nanoreplicas are shown in Figure S5. To clarify, the initial catalytic performance of the chromium oxide-based catalysts (with Cr$_2$O$_3$ loading of 20 wt %) deposited on other mesoporous supports was reported as well. The Cr20/Al$_2$O$_3$-n catalyst exhibits better catalytic performance than Cr20/SBA-15 and Cr20/MCM-41, but lower performance in comparison to Cr20/CMK-3. However, in the latter case, the great limitation is catalyst regeneration because the CMK-3 support cannot be regenerated in an air flow.

Table 3. Initial catalytic performances in dehydrogenation of propane to propene [a].

Sample	Temp. (°C)	Conversion (%)	Yield (%)		Selectivity (%)		
		C$_3$H$_8$	C$_3$H$_6$	C$_3$H$_6$	C$_2$H$_6$	C$_2$H$_4$	CH$_4$
Cr1/Al$_2$O$_3$-n	550	13.0	10.4	79.9	1.4	12.1	6.6
Cr5/Al$_2$O$_3$-n	550	21.9	19.4	88.8	2.3	5.1	3.9
Cr10/Al$_2$O$_3$n	550	24.6	22.8	92.3	1.6	2.9	3.2
Cr20/Al$_2$O$_3$-n	500	12.9	11.3	87.7	1.8	5.2	5.3
	550	33.8	31.7	94.0	1.4	2.1	2.4
	600	41.8	37.5	89.8	2.3	3.9	3.9
Cr30/Al$_2$O$_3$-n	550	17.8	17.5	98.2	0.3	0.4	0.2
Cr20/SBA-15	550	25.7	22.1	86.0	4.8	2.7	5.6
Cr20/MCM-41	550	28.9	24.9	86.0	4.0	4.6	5.4
Cr20/CMK-3 [b]	550	47.4	40.1	84.7	3.3	3.8	8.4

[a] Reaction conditions: Weight hourly space velocity WHSV = 1.2 h^{-1}; C$_3$H$_8$:He molar ratio = 1:14; Total flow rate = 30 cm^3·min^{-1}; Catalyst weight = 200 mg; Results are summarized after 10 min-on-stream. [b] from [37].

It is clear that the conversion of propane and the yield of propylene achieved at 550 °C rise with the increase in the Cr loading up to 20 wt % and then decline. In this regard, the Crx/Al$_2$O$_3$-n samples exhibit similar catalytic behavior to other Cr-containing materials deposited on oxide supports, such as SiO$_2$ [32], SBA-15 [31,32], SBA-1 [9,28], ZrO$_2$ [29], or Al$_2$O$_3$ [30]. Typically, over supported chromium oxide catalysts, prepared by impregnation, the catalytic activity in the dehydrogenation of hydrocarbons increases with a Cr loading reaching an optimal value. A further increase in the Cr content results in a decrease in the catalytic activity mainly due to pore clogging and/or formation α-Cr$_2$O$_3$ that is a less active phase [32]. The loading needed to achieve the maximum of catalytic performance changes in a wide ranges from 5 to 20 wt % and depends on synthesis conditions, kind of precursors and nature of support (textural parameters as well as phase and chemical composition). As we reported in previous works [28,32], over silica-supported chromium oxide catalyst activity in the PDH process correlates well with the number of redox Cr species in the fresh or regenerated catalysts. These sites are reduced during the initial step of PDH to catalytically active coordinatively unsaturated Cr species.

Figure 4 illustrates variations of specific activity and rate of propylene formation in the PDH process as well as the percent of redox and non-redox in nature Cr sites with the total Cr concentration in the catalyst. The catalytic activity drops rapidly with an increase in the total Cr content (Figure 4B). A similar decrease is observed in mole percent of Cr redox species (Figure 4A) and confirms that this type of sites is crucial for high activity. The propylene formation rate normalized to 1 g of a catalyst rises almost proportionally with the Cr concentration below monolayer coverage that for an alumina

support is between 3.7 and 4.5 Cr at. nm^{-1} according to different sources [30,40]. After exceeding the monolayer coverage, the formation rate increases slowly with a Cr loading. This effect can be related to the formation of small particles of Cr_2O_3 detected by UV-Vis DRS (band at 600 nm) and EPR (β-signal). The highest formation rate is achieved over the catalyst with 6.6 Cr at. nm^{-1} (20 wt % of Cr_2O_3). In this catalyst, the contribution of Cr redox species is only 18%. Above this concentration of Cr the formation rate declines rapidly. As was pointed above, the drop in activity correlates well with the appearance of α-Cr_2O_3 crystals located outside of the mesopore systems. These much larger crystallites present low catalytic activity.

Taking into account a contribution of redox Cr species in the catalytic activity, the changes in the oxidation state of Cr were studied during the PDH process by UV-Vis-DRS. The operando experiments were carried over two Crx/Al_2O_3-n samples, e.g., $Cr1/Al_2O_3$-n enriched in the Cr redox species and $Cr20/Al_2O_3$-n, with a large number of non-redox Cr species.
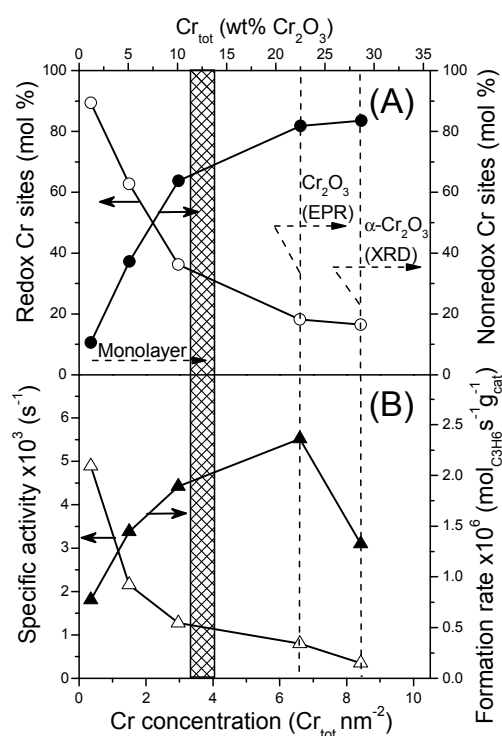

Figure 4. Variation of mole percent of redox and non-redox in origin Cr species (**A**) as well as specific activity and formation rate (**B**) with total Cr concentration. Reaction conditions: T = 550 °C; $m_{cat.}$ = 200 mg; Feed gas composition C_3H_8:He =1:14; Total flow rate = 30 $cm^3 \cdot min^{-1}$; WHSV = 1.2 h^{-1}; Results collected after 10 min-on-stream.

Figure 5 shows UV-Vis-DR spectra recorded in the range of 250–1000 nm during the PDH process performed at 550 °C. For separation of the initial reduction and deactivation steps the spectra were divided into two ranges: (1) 0–10 min-on-stream, and (2) 10–240 min-on-stream. In the initial step of the PDH process, fast changes in intensity and shape of bands occur due to the reduction of Cr(VI) species. For both samples, the intensity of band in the CT range (about 360–380 nm) drops, while the new broad band appears at about 650–700 nm, evidencing the formation of Cr(III) species. However, in the case of $Cr20/Al_2O_3$-n, the tracking of Cr oxidation state is more complicated due to the high surface Cr concentration (weak signal in diffuse reflectance mode) and fast changes of the catalyst color (darkening) caused by carbon deposit. The deactivation of the catalysts by the coke can be more clearly observed between 10 and 240 min-on-stream (Figure 5B,D). In this period, the intensity of background, related to deactivation by coke, grows for both investigated catalysts.
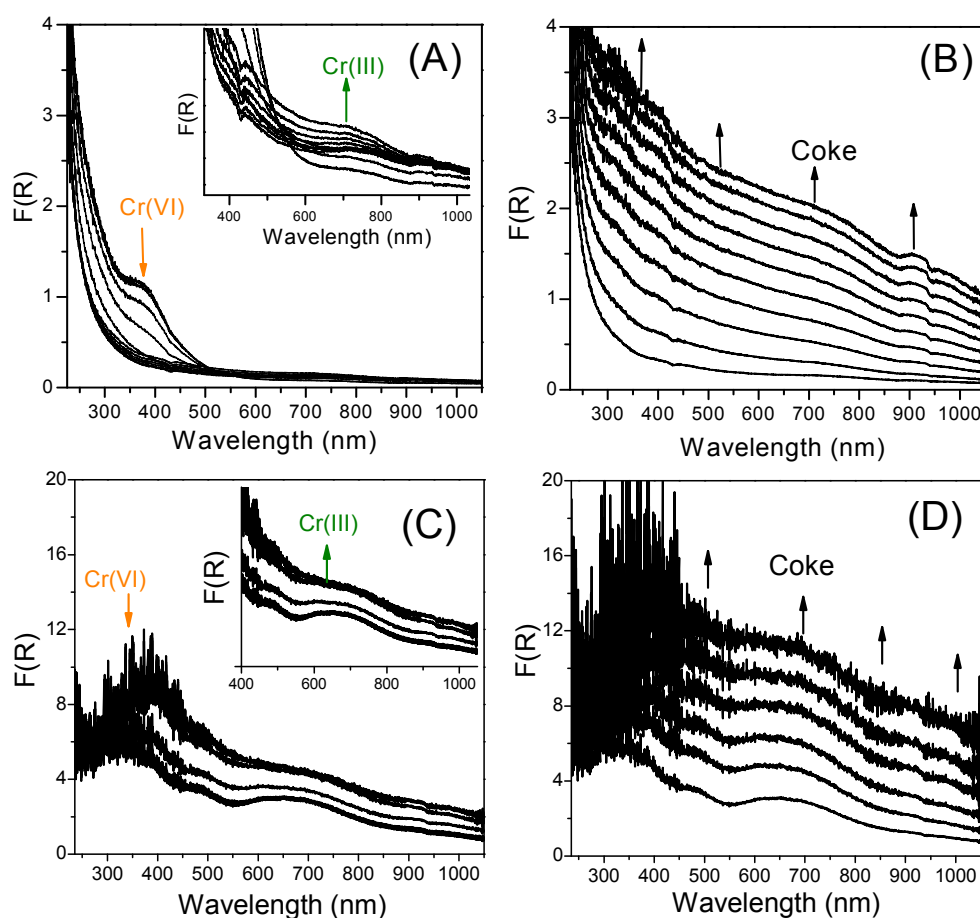
Figure 5. UV-Vis DRS spectra recorded during first 10 min (**A**,**C**) and between 10 and 240 min (**B**,**D**) of process over the Cr1/Al$_2$O$_3$-n and Cr20/Al$_2$O$_3$-n catalysts. Reaction conditions: T = 550 °C; m$_{cat.}$ = 200 mg; WHSV = 1.2 h^{-1}; Feed gas composition C$_3$H$_8$:He =1:14; Total flow rate = 30 cm$^3 \cdot$min^{-1}.

It should be noted that in the case of alumina-supported chromium catalysts, the nature (redox and non-redox) and nucleation of the active Cr(III) sites are still subject of discussion [23,24,30,41]. The content of redox and non-redox Cr sites as well as their nucleation varies with preparation procedures, origin of alumina and Cr content, therefore the estimation of which of the Cr(III) sites exhibits the highest activity and the contribution in the PDH is difficult. In the case of our mesoporous catalysts, a good proportion between the number of redox sites and the catalytic performance in PDH is observed with the low Cr content where on the surface of the catalysts almost selectively redox species existed (89 mol %). However, the percent of redox species rapidly decreases with the Cr content indicating a rise in the content of non-redox Cr species contribution at the high Cr loadings. The letter species seem to play an important role in the catalysts containing 20 wt % of Cr$_2$O$_3$ over which the highest rate of propylene formation is observed.

2.3.2. Effect of Support

An effect of nanocasting on the catalytic performance of the chromium oxide-based materials supported on Al$_2$O$_3$-n (calcined at 700 °C) obtained by nanoreplication and commercially available Al$_2$O$_3$-c was studied. Both the catalysts were prepared by an identical preparation procedure and contained the same intended amount of chromium (20 wt %), that was close to concentration of Cr in the industrial catalysts for the dehydrogenation of light alkanes used in the CATOFIN process [3].

Table S1 summarizes base characterization of pure Al$_2$O$_3$-c. The commercial Al$_2$O$_3$-c support has a lower specific surface area (S$_{BET}$ = 161 m$^2 \cdot$g^{-1}) and porosity (V$_{tot}$ = 0.24 cm$^3 \cdot$g^{-1}) than Al$_2$O$_3$-n

(Table 1). Moreover, Al_2O_3-c is characterized by slightly higher total acidity in comparison with Al_2O_3-n and both supports have similar medium–strong acidity. Total and medium–strong acidity estimated based on NH_3-TPD for pure Al_2O_3-c are 2.01 and 1.43 µmol $NH_3 \cdot m^{-2}$, while in the case of Al_2O_3-n these values are 1.86 and 1.46 µmol $NH_3 \cdot m^{-2}$, respectively.

Figure 6 shows variation of propene yield vs. time-on-stream (TOS) and thermogravimetric method (TG) profiles of used catalysts. At 500 °C the $Cr20/Al_2O_3$-c and $Cr20/Al_2O_3$-n catalysts exhibited a similar catalytic performance. A difference in the catalytic behavior between both investigated catalysts was revealed at higher temperatures. In the PDH process carried out at 550 and 600 °C the higher initial yield of propene was achieved over the $Cr20/Al_2O_3$-c catalyst. However, this catalyst deactivated faster in comparison with $Cr20/Al_2O_3$-n. After 30–60 min on-stream the yield of propene obtained over $Cr20/Al_2O_3$-n was higher at both studied temperatures. A comparison of the TG profiles of both catalysts reveals a difference in loss of weight only at 550 and 600 °C. In the mentioned temperatures higher loss of weight is observed in the case of $Cr20/Al_2O_3$-c indicating larger amount of deposited coke. Assuming that both alumina supports have similar medium–strong acidity, it can be proposed that the observed differences in the catalytic behavior and coke amount are related to porosity. A slower deactivation of the catalysts, based on the Al_2O_3-n nanoreplica, is probably connected with its higher specific surface area and ordered mesoporous arrangement forced by using the hard template.
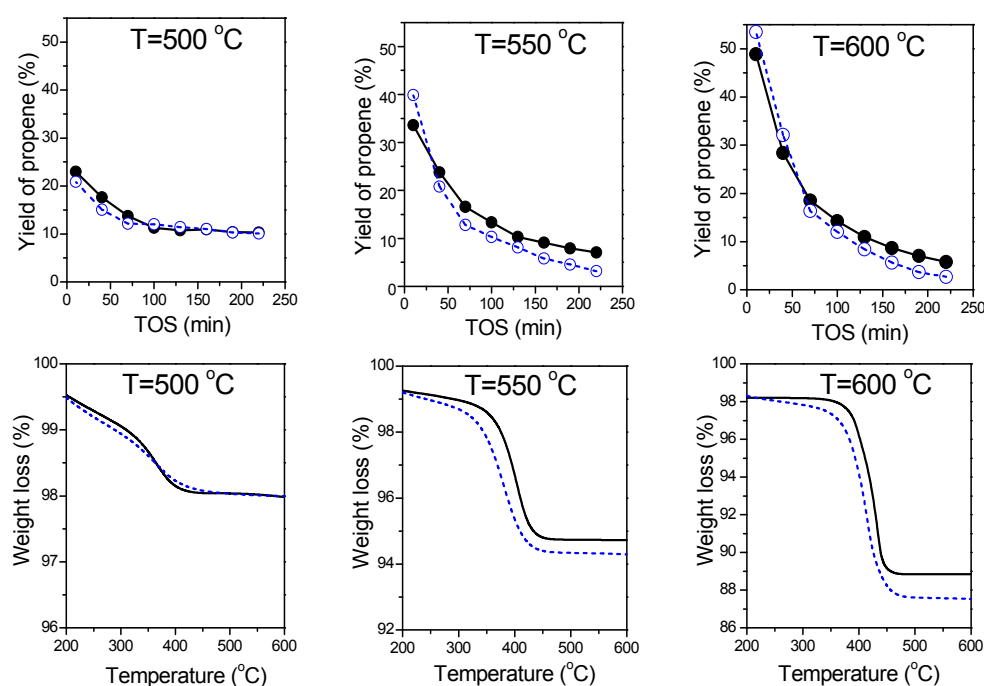

Figure 6. Comparison of $Cr20/Al_2O_3$-n (solid line) and $Cr20/Al_2O_3$-c (dot line) catalysts stability during PDH at 500. 550 and 600 °C. Reaction conditions: $m_{cat.}$ = 200 mg; Feed gas composition C_3H_8:He = 1:14; Total flow rate = 30 $cm^3 \cdot min^{-1}$; WHSV = 1.2 h^{-1}.

2.3.3. Regeneration Behavior

Finally, the stability of the $Cr20/Al_2O_3$-n catalyst in several dehydrogenation-regeneration cycles was studied. Figure 7 presents the variations in the conversion of propane, yield and selectivity to propene in the consecutive dehydrogenation steps. In each PDH step, the catalyst lost its activity due to the coke formation.
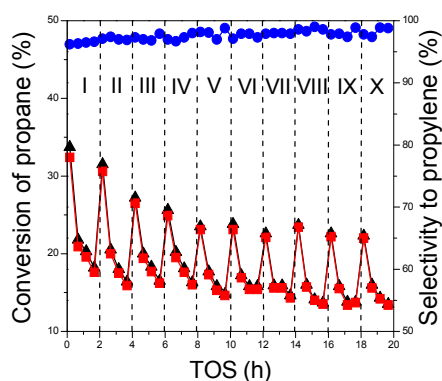
Figure 7. Variation of propane conversion (▲). propene yield (■) and selectivity (●) with time-on-stream in consecutive I–X cycles over Cr20/Al$_2$O$_3$-n. Dehydrogenation conditions: reaction temperature = 550 °C; catalyst weight = 200 mg; feed gas composition C$_3$H$_8$:He = 1:14; total flow rate = 30 cm^3·min^{-1}. Regeneration conditions: temperature = 550 °C; total flow rate of air = 30 cm^3·min^{-1}. Purification conditions: temperature = 550 °C; total flow rate of helium = 30 cm^3·min^{-1}. TOS: time-on-stream.

After regeneration in the flow of air, the catalytic performance is partially restored. In the first four cycles the initial conversion of propane and the initial yield of propylene decreased by 3–5% in the consecutive PDH steps. A similar behavior of other PDH catalysts based on mesoporous supports, such as CrOx/SBA-1 or VOx/Al$_2$O$_3$, was discussed earlier [9,10,28]. Typically, the irreversible initial deactivation in the consecutive PDH cycles is caused either by structural changes of active species (such as agglomeration) or loss of regularity of mesoporous support.

In the case of the Cr20/Al$_2$O$_3$-n catalyst, after an initial period (four cycles) the catalytic performance in the further consecutive PDH cycles showed only insignificant differences, demonstrating good long-term stability.

3. Materials and Methods

3.1. Catalyst Preparation

SBA-15 silica was synthesized in 2 M HCl solution using Pluronic P123 (EO20PO70EO20, Mav = 5800, Aldrich, St. Louis, MO, USA) as a template and tetraethylorthosilicate (98%, Aldrich, Shanghai, China) as a silica source. CMK-3 carbon was prepared using SBA-15 as a template and an aqueous solution of sucrose as a precursor of carbon [37,42].

Mesoporous Al$_2$O$_3$ support (denoted as Al$_2$O$_3$-n) was obtained by the incipient wetness impregnation method according to the procedure reported elsewhere [37]. In the typical synthesis, the CMK-3 was impregnated twice using a 1 M aqueous solution of Al(NO$_3$)$_3$ (99.96 wt %, Aldrich, Steinheim, Germany). In the first and second impregnations volumes of 4.0 and 3.2 cm^3 of solution per 1 g of CMK-3 were used, respectively. After each impregnation step, the material was heated to 250 °C at a constant rate of 1 °C·min^{-1}. Finally, the material was calcined in two steps. An inert gas (N$_2$) atmosphere was obtained by raising the temperature from ambient-level to 600 °C at a rate of 1 °C·min^{-1}, followed by maintenance of the final temperature for another 10 h. After cooling to room temperature, the sample was heated again in a flow of air using the same program, but with final temperatures of 600, 700, 800 and 900 °C, respectively.

Crx/Al$_2$O$_3$-n catalysts were prepared by the incipient wetness method using Cr(NO$_3$)$_3$·9H$_2$O (99.6 wt %, Polish Chemical Reagents, Gliwice, Poland) as a chromium source. The support (1 g of Al$_2$O$_3$-n) was treated with 3.0 cm^3 of an aqueous solution of Cr(NO$_3$)$_3$. The concentration of Cr(NO$_3$)$_3$ in solution was matched so as to obtain 1, 5, 10, 20 and 30 wt % of the total Cr$_2$O$_3$ content (Cr$_{tot}$.) in the catalysts. The samples were dried overnight at room temperature, then kept at 60 °C for 6 h, and

finally calcined at 600 °C for 6 h in a flow of air. The catalysts were denoted as Crx/Al_2O_3-n, where x stands for nominal Cr_{tot} given in wt % of Cr_2O_3.

According to the same procedure, a reference catalyst was prepared using commercial γ-Al_2O_3 (Aldrich, Steinheim, Germany). Before impregnation, the support was calcined at 700 °C for 6 h in an air flow. The catalyst was prepared by impregnation of the alumina support with an aqueous solution of chromium nitrate (to obtain 20 wt % of Cr_2O_3 loading in the final samples) followed by thermal decomposition as in the case of the Crx/Al_2O_3-n series. The catalyst was designated as $Cr20/Al_2O_3$-c.

3.2. Characterization Techniques

The total Cr content (Cr_{tot}) in the samples (after mineralization) was determined using inductively-coupled plasma optical emission spectrometry (ICP-OES). An Optima 2100 DV spectrometer (Perkin-Elmer, Shelton, CT, USA) was used for the determination of Cr at the wavelength of λ_{Cr} = 267.716 nm. In the typical mineralization procedure, a sample (ca. 50 mg) was mixed with 2 g of $NaNO_3$ (POCh-Polish Chemical Reagents, Gliwice, Poland) and 2 g of NaOH (POCh-Polish Chemical Reagents, Gliwice, Poland) in a melting pot. Then, the mixture was heated to 600 °C in air. The mineralization mixture was cooled to room temperature, dissolved in deionized water and filtered. Cr_{tot} was determined in a dissolved solution.

Temperature-programmed reduction (H_2-TPR) and ammonia desorption (NH_3-TPD) experiments were carried out in a modified gas chromatograph equipped with a thermal conductivity detector connected with a quartz reactor. In the TPR experiments, the mixture of N_2/H_2 (95/5 vol %, Air Liquide, Kraków, Poland) served as a combined carrier and reducing gas at a total flow rate of 30 $cm^3 \cdot min^{-1}$. Before the H_2-TPR experiments, the samples were dried at 120 °C for 12 h. The catalyst (50 mg) was preheated in the reactor in helium (99.999 vol %, Linde Gaz Polska, Kraków, Poland) at 600 °C for 30 min, and then cooled down to room temperature (RT) in the He stream. During the H_2-TPR experiments, the temperature was raised from RT to 600 °C at the rate of 10 $°C \cdot min^{-1}$. The H_2 consumption was measured by thermal conductivity detector (TCD) after removal of water vapor by condensation. Ultra-pure NiO (99.999%, Aldrich) was used as a standard for calibration.

In the TPD experiments, a 100 mg sample was preheated in He at 600 °C for 2 h and then equilibrated with NH_3 (99.98 vol.%, Linde Gaz Polska, Kraków, Poland) at room temperature. Physisorbed NH_3 was removed by purging with pure He at 100 °C for 2 h. The TPD measurement was conducted by heating the sample from 100 to 700 °C at the rate of 10 $°C\ min^{-1}$ in pure helium (30 $cm^3 \cdot min^{-1}$).

Low-temperature nitrogen adsorption–desorption isotherms were measured at -196 °C using a ASAP 2020 instrument (Micromeritics, Norcross, GA, USA). Before the measurements, the samples were degassed at 250 °C for 12 h. Specific surface areas (S_{BET}) were calculated using the Brunauer–Emmett–Teller method within the relative pressure of P/P_0 = 0.05–0.15. Pore size distributions were calculated from the desorption branches of the isotherms using the Barrett–Joyner–Halenda (BJH) model. Total pore volumes were obtained from the volumes of nitrogen adsorbed at P/P_0 about 0.97.

XRD patterns were collected on a D2 Phaser diffractometer (Bruker, Madison, WI, USA) operated at 40 kV and 30 mA, equipped with a Cu K_α X-ray radiation (λ = 0.154 nm) with a step size of 0.02°.

Electron paramagnetic resonance (EPR) spectra were recorded at RT with a X-band Bruker ELEXSYS-580 spectrometer operating at 100 kHz field modulation with 1–5 G modulation amplitude. Morphology and structure of solids were investigated by means of a JEOL JSM-7500F field emission scanning electron microscope equipped with a transmission electron microscopy detector TED (total energy *detector*). In SEM experiments, catalysts were deposited on a sample holder. K575X Turbo Sputter Coater was used for coating the specimens with gold (deposited film thickness—20 nm). The specimens for the TEM study were prepared by depositing a small amount of powder samples on holey carbon films supported on copper grids.

Samples after a catalytic run in the PDH process were analyzed by thermogravimetric method (TG) in flowing air (100 cm^3/min) using a SDT Q600 apparatus (TA Instruments, New Castle, DE, USA). A sample (ca. 5 mg) was placed in a crucible and heated to 900 °C at a rate of 20 °C/min.

3.3. Catalytic Tests

The catalytic performance of the synthesized samples was investigated in the dehydrogenation of propane to propene. The process was carried out in a tubular stainless-still reactor (SS316, i.d. 9.1 mm) packed with 200 mg of a catalyst (grain size 0.2–0.3 mm) in the temperature range of 500–600 °C and under atmospheric pressure using PID Microactivity-XS15. Before the PDH process, the sample was preheated at 600 °C for 30 min in an air flow and then for another 30 min in a dry He stream. After that, the reaction temperature was set and after stabilization time an inert gas (He) was replaced with a mixture of propane (99.96% Linde) diluted with He (99.9996% Linde, Gaz Polska, Kraków, Poland) 2/28 *vol./vol.* at the total flow rate of 30 cm^3·min^{-1} (WHSV = 1.2 h^{-1}). The products and unreacted substrates were analyzed using an Agilent 6890N gas chromatograph (equipped with Hayesep Q and 13X molecular sieves packed columns and TCD), connected with the reactor. Specific activity, rate of propene formation (activity), conversion of propane, yield of propene and selectivity to all hydrocarbon products were calculated based on carbon balance in inlet and outlet of the microreactor using the equations reported elsewhere [42].

3.4. Operando UV-Vis DRS

During selected PDH tests, the oxidation state of chromium species on the surface of alumina was monitored by operando UV-Vis-DR spectroscopy using Ocean Optics HR2000+ (integration time 20 msec, 20 scans, Winter Park, FL, USA) equipped with an Ocean Optics DH-2000 BAL (Ostfildern, German) halogen-deuterium light source and a FCR-7UV400-2-ME-HTX reflection probe (7 × 400 µm fibers, Anglia Instrument Ltd, Cambridgeshire, UK). The spectra were collected in the wavelength range of 225–1100 nm using BaSO$_4$ as a reflection standard. The spectra are shown in the Kubelka–Munk format (F(R) = (1 − R)2/2R; where R stands for reflectance). The probe was attached at the top of the quartz microreactor within a distance of 2–3 mm from the catalyst bed of 4–5 mm thickness.

4. Conclusions

Nanoreplication provides the possibility of obtaining thermally stable (up to 700 °C) mesoporous alumina support with ordered pore arrangement and specific surface as high as 270 m^2/g. Based on this support Cr-containing catalysts for the PDH process can be obtained by impregnation with various amounts of chromium oxide active phase. The optimal propene yield of 32% was reached at 550 °C in the sample containing 20 wt % of Cr$_2$O$_3$. In the studied catalysts both redox and non-redox Cr species coexist. The concentration of the redox sites in respect to the non-redox ones decreases with the total Cr content. The Cr(V) and Cr(VI) species present in the fresh or regenerated catalysts are the precursors of redox Cr(III) species that are formed in the initial period of the dehydrogenation process. These species seem to be responsible for the catalytic activity at a low Cr content, while at higher Cr loadings both redox and non-redox in origin Cr(III) species influence the catalytic activity. A comparative investigation of chromium oxide-based materials supported on nanocasted and commercial alumina revealed that the former samples had better resistance to deactivation.

Author Contributions: P.M. and P.K. conceived and designed the experiments; A.W. (Węgrzyniak) carried out catalytic tests for the prepared nanoreplicas; S.J. performed XRD and TGA–DTA analyses; A.W. (Węgrzynowicz) performed N_2-sorption; B.M. performed temperature-programmed experiments; P.K. analyzed the XRD and TGA data and participated in interpretation and discussion of the results collected at all stages of investigation; and P.M. performed operando UV-Vis DRS experiments and wrote the manuscript.

Conflicts of Interest: The authors declare no conflict of interest.

References

1. Bhasin, M.M.; McCain, J.H.; Vora, B.V.; Imai, T.; Pujadó, P.R. Dehydrogenation and oxydehydrogenation of paraffins to olefins. *Appl. Catal. A Gen.* **2001**, *221*, 397–419. [CrossRef]

2. Cavani, F.; Ballarini, N.; Cericola, A. Oxidative dehydrogenation of ethane and propane: How far from commercial implementation? *Catal. Today* **2007**, *127*, 113–131. [CrossRef]

3. Sattler, J.J.H.B.; Ruiz-Martinez, J.; Santillan-Jimenez, E.; Weckhuysen, B.M. Catalytic dehydrogenation of light alkanes on metals and metal oxides. *Chem. Rev.* **2014**, *114*, 10613–10653. [CrossRef] [PubMed]

4. Sanfilippo, D. Dehydrogenation of Paraffins; Key Technology for Petrochemicals and Fuels. *Cattech* **2000**, *4*, 56–73. [CrossRef]

5. Michorczyk, P.; Ogonowski, J.; Kuśtrowski, P.; Chmielarz, L. Chromium oxide supported on MCM-41 as a highly active and selective catalyst for dehydrogenation of propane with CO_2. *Appl. Catal. A Gen.* **2008**, *349*, 62–69. [CrossRef]

6. Liu, L.; Li, H.; Zhang, Y. Mesoporous silica-supported chromium catalyst: Characterization and excellent performance in dehydrogenation of propane to propylene with carbon dioxide. *Catal. Commun.* **2007**, *8*, 565–570. [CrossRef]

7. Botavina, M.A.; Martra, G.; Agafonov, Y.A.; Gaidai, N.A.; Nekrasov, N.V.; Trushin, D.V.; Coluccia, S.; Lapidus, A.L. Oxidative dehydrogenation of C_3-C_4 paraffins in the presence of CO_2 over CrO_x/SiO_2 catalysts. *Appl. Catal. A Gen.* **2008**, *347*, 126–132. [CrossRef]

8. Ohishi, Y.; Kawabata, T.; Shishido, T.; Takaki, K.; Zhang, Q.; Wang, Y.; Takehira, K. Dehydrogenation of ethylbenzene with CO_2 over Cr-MCM-41 catalyst. *J. Mol. Catal. A Chem.* **2005**, *230*, 49–58. [CrossRef]

9. Michorczyk, P.; Ogonowski, J.; Niemczyk, M. Investigation of catalytic activity of CrSBA-1 materials obtained by direct method in the dehydrogenation of propane with CO_2. *Appl. Catal. A Gen.* **2010**, *374*, 142–149. [CrossRef]

10. Bai, P.; Ma, Z.; Li, T.; Tian, Y.; Zhang, Z.; Zhong, Z.; Xing, W.; Wu, P.; Liu, X.; Yan, Z. Relationship between Surface Chemistry and Catalytic Performance of Mesoporous γ-Al_2O_3 Supported VO_X Catalyst in Catalytic Dehydrogenation of Propane. *ACS Appl. Mater. Interfaces* **2016**, *8*, 25979–25990. [CrossRef] [PubMed]

11. Sokolov, S.; Stoyanova, M.; Rodemerck, U.; Linke, D.; Kondratenko, E.V. Effect of support on selectivity and on-stream stability of surface VOx species in non-oxidative propane dehydrogenation. *Catal. Sci. Technol.* **2014**, *4*, 1323–1332. [CrossRef]

12. Sokolov, S.; Bychkov, V.Y.; Stoyanova, M.; Rodemerck, U.; Bentrup, U.; Linke, D.; Tyulenin, Y.P.; Korchak, V.N.; Kondratenko, E.V. Effect of VOx species and support on coke formation and catalyst stability in nonoxidative propane dehydrogenation. *ChemCatChem* **2015**, *7*, 1691–1700. [CrossRef]

13. Michorczyk, P.; Ogonowski, J. Dehydrogenation of propane to propene over gallium oxide in the presence of CO_2. *Appl. Catal. A Gen.* **2003**, *251*, 425–433. [CrossRef]

14. Zheng, B.; Hua, W.; Yue, Y.; Gao, Z. Dehydrogenation of propane to propene over different polymorphs of gallium oxide. *J. Catal.* **2005**, *232*, 143–151. [CrossRef]

15. Tan, S.; Hu, B.; Kim, W.G.; Pang, S.H.; Moore, J.S.; Liu, Y.; Dixit, R.S.; Pendergast, J.G.; Sholl, D.S.; Nair, S.; et al. Propane Dehydrogenation over Alumina-Supported Iron/Phosphorus Catalysts: Structural Evolution of Iron Species Leading to High Activity and Propylene Selectivity. *ACS Catal.* **2016**, *6*, 5673–5683. [CrossRef]

16. Michorczyk, P.; Kuśtrowski, P.; Chmielarz, L.; Ogonowski, J. Influence of redox properties on the activity of iron oxide catalysts in dehydrogenation of propane with CO_2. *React. Kinet. Catal. Lett.* **2004**, *82*, 121–130. [CrossRef]

17. Yun, Y.; Araujo, J.R.; Melaet, G.; Baek, J.; Archanjo, B.S.; Oh, M.; Alivisatos, A.P.; Somorjai, G.A. Activation of Tungsten Oxide for Propane Dehydrogenation and Its High Catalytic Activity and Selectivity. *Catal. Lett.* **2017**, *147*, 622–632. [CrossRef]

18. Chen, M.; Xu, J.; Gao, Y.; He, H.-Y.; Fan, K.-N.; Zhuang, J.-H. Dehydrogenation of propane over In_2O_3–Al_2O_3 mixed oxide in the presence of carbon dioxide. *J. Catal.* **2010**, *272*, 101–108. [CrossRef]

19. Gaspar, A.B.; Brito, J.L.F.; Dieguez, L.C. Characterization of chromium species in catalysts for dehydrogenation and polymerization. *J. Mol. Catal. A Chem.* **2003**, *203*, 251–266. [CrossRef]

20. Mentasty, L.R.; Gorriz, O.F.; Cadus, L.E. Chromium Oxide Supported on Different Al_2O_3 Supports: Catalytic Propane Dehydrogenation. *Ind. Eng. Chem. Res.* **1999**, *38*, 396–404. [CrossRef]

21. Cherian, M.; Rao, M.S.; Hirt, A.M.; Wachs, I.E.; Deo, G. Oxidative dehydrogenation of propane over supported chromia catalysts: Influence of oxide supports and chromia loading. *J. Catal.* **2002**, *211*, 482–495. [CrossRef]

22. Airaksinen, S.M.K.; Krause, A.O.I. Effect of catalyst prereduction on the dehydrogenation of isobutane over chromia/alumina. *Ind. Eng. Chem. Res.* **2005**, *44*, 3862–3868. [CrossRef]

23. Santhosh Kumar, M.; Hammer, N.; Rønning, M.; Holmen, A.; Chen, D.; Walmsley, J.C.; Øye, G. The nature of active chromium species in Cr-catalysts for dehydrogenation of propane: New insights by a comprehensive spectroscopic study. *J. Catal.* **2009**, *261*, 116–128. [CrossRef]

24. Puurunen, R. Spectroscopic Study on the Irreversible Deactivation of Chromia/Alumina Dehydrogenation Catalysts. *J. Catal.* **2002**, *210*, 418–430. [CrossRef]

25. Cherian, M.; Someswara, M.; Yang, W.; Jehng, J.; Hirt, A.M.; Deo, G. Oxidative dehydrogenation of propane over Cr_2O_3/Al_2O_3 and Cr_2O_3 catalysts: Effects of loading, precursor and surface area. *Appl. Catal. A Gen.* **2002**, *233*, 21–33. [CrossRef]

26. Gaspar, A.B.; Dieguez, L.C. Distribution of chromium species in catalysts supported on ZrO_2/Al_2O_3 and performance in dehydrogenation. *J. Catal.* **2003**, *220*, 309–316. [CrossRef]

27. Nijhuis, T.A.; Tinnemans, S.J.; Visser, T.; Weckhuysen, B.M. Towards real-time spectroscopic process control for the dehydrogenation of propane over supported chromium oxide catalysts. *Chem. Eng. Sci.* **2004**, *59*, 5487–5492. [CrossRef]

28. Michorczyk, P.; Pietrzyk, P.; Ogonowski, J. Preparation and characterization of SBA-1-supported chromium oxide catalysts for CO_2 assisted dehydrogenation of propane. *Microporous Mesoporous Mater.* **2012**, *161*, 56–66. [CrossRef]

29. De Rossi, S.; Casaletto, M.P.; Ferraris, G.; Cimino, A.; Minelli, G. Chromia/zirconia catalysts with Cr content exceeding the monolayer. A comparison with chromia/alumina and chromia/silica for isobutane dehydrogenation. *Appl. Catal. A Gen.* **1998**, *167*, 257–270. [CrossRef]

30. Hakuli, A.; Kytökivi, A.; Krause, A.O.I. Dehydrogenation of i-Butane on $CrOx$/Al_2O_3 Catalysts Prepared by ALE and Impregnation Techniques. *Appl. Catal. A Gen.* **2000**, *190*, 219–232. [CrossRef]

31. Zhang, X.; Yue, Y.; Gao, Z. Chromium oxide supported on mesoporous SBA-15 as propane dehydrogenation and oxidative dehydrogenation catalysts. *Catal. Lett.* **2002**, *83*, 19–25. [CrossRef]

32. Michorczyk, P.; Ogonowski, J.; Zeńczak, K. Activity of chromium oxide deposited on different silica supports in the dehydrogenation of propane with CO_2—A comparative study. *J. Mol. Catal. A Chem.* **2011**, *349*, 1–12. [CrossRef]

33. Vaudry, F.; Khodabandeh, S.; Davis, M.E. Synthesis of Pure Alumina Mesoporous Materials. *Chem. Mater.* **1996**, *8*, 1451–1464. [CrossRef]

34. Liu, Q.; Wang, A.; Xu, J.; Zhang, Y.; Wang, X.; Zhang, T. Preparation of ordered mesoporous crystalline alumina replicated by mesoporous carbon. *Microporous Mesoporous Mater.* **2008**, *116*, 461–468. [CrossRef]

35. Liu, Q.; Wang, A.; Wang, X.; Zhang, T. Ordered crystalline alumina molecular sieves synthesized via a nanocasting route. *Chem. Mater.* **2006**, *18*, 5153–5155. [CrossRef]

36. Haffer, S.; Weinberger, C.; Tiemann, M. Mesoporous Al_2O_3 by nanocasting: Relationship between crystallinity and mesoscopic order. *Eur. J. Inorg. Chem.* **2012**, 3283–3288. [CrossRef]

37. Michorczyk, P.; Kuśtrowski, P.; Kolak, A.; Zimowska, M. Ordered mesoporous Ga_2O_3 and Ga_2O_3-Al_2O_3 prepared by nanocasting as effective catalysts for propane dehydrogenation in the presence of CO_2. *Catal. Commun.* **2013**, *35*, 95–100. [CrossRef]

38. Weckhuysen, B.M.; Verberckmoes, A.A.; De Baets, A.R.; Schoonheydt, R.A. Diffuse reflectance spectroscopy of supported chromium oxide catalysts: A self-modeling mixture analysis. *J. Catal.* **1997**, *166*, 160–171. [CrossRef]

39. Weckhuysen, B.M.; Wachs, I.E.; Schoonheydt, R.A. Surface Chemistry and Spectroscopy of Chromium in Inorganic Oxides. *Chem. Rev.* **1996**, *96*, 3327–3350. [CrossRef] [PubMed]

40. Wachs, I.E.; Deo, G.; Vuurman, M.A.; Hu, H.; Kim, D.S.; Jehng, J.-M. Molecular design of supported metal oxide catalysts: An initial step to theoretical models. *J. Mol. Catal.* **1993**, *82*, 443–455. [CrossRef]

41. Hakuli, A.; Harlin, M.E.; Backman, L.B.; Krause, A.O.I. Dehydrogenation of i-Butane on CrO_x/SiO_2 Catalysts. *J. Catal.* **1999**, *184*, 349–356. [CrossRef]

42. Węgrzyniak, A.; Jarczewski, S.; Wach, A.; Hędrzak, E.; Kuśtrowski, P.; Michorczyk, P. Catalytic behaviour of chromium oxide supported on CMK-3 carbon replica in the dehydrogenation propane to propene. *Appl. Catal. A Gen.* **2015**, *508*, 1–9. [CrossRef]